

A Method for Proton Detector Efficiency Measurement with Applications in Neutron Beta Decay and Lifetime Experiments

Grant V. Riley^c, Nadia Fomin^{a,*}, Jaideep Taggart Singh^b, William Greene^a,
Rebecca Godri^a, Evan Adamek^a, Eli Carter^a

^a*University of Tennessee, Knoxville*

^b*640 S. Shaw Lane, Facility for Rare Isotope Beams, Michigan State University*

^c*Los Alamos National Laboratory*

Abstract

This article proposes a new method to measure the proton detector efficiency for use in “beam” determinations of the free neutron lifetime. There is currently a 4σ disagreement between the “beam” and “storage” methods of measuring the lifetime of the neutron. A possible reason for this is a systematic uncertainty that is not properly accounted for in one or both types of experiments. Absolute proton counting is an essential facet of the “beam” experimental approach. The absolute detector efficiency is not currently known for existing experiments and could be a source of a hidden systematic error. The proposed absolute calibration techniques can also be extended to new, large area particle detectors designed for future experiments. We propose to laser ionize a beam of atomic hydrogen and simultaneously count both the outgoing protons and electrons. Due to recent advances in UV laser and atomic hydrogen beam technologies, we estimate a count rate as high as $\sim 200\text{k}$ proton-electrons pairs per second under the most favorable scheme discussed. Our proposed technique would remove one of the leading systematic uncertainties in the determination of the neutron lifetime, making an precision of ± 0.16 s feasible. Precise and accurate knowledge of the proton detection efficiency is crucial to fully understanding the systematics of the “beam” measurement method as well as developing next

*Corresponding Author

generation experiments that will have the precision to test the Standard Model.

Keywords: neutron physics, neutron lifetime, detector efficiency

1. Motivation

Neutron beta decay is a process that has been under investigation since the discovery of the neutron in the early 1930s. However, even today, the free neutron lifetime is not known to a satisfactory level of accuracy [1, 2]. The neutron lifetime is an input to Big Bang Nucleosynthesis calculations which determine light element abundances in the early universe [3, 4, 5] and the uncertainty on the lifetime is the most significant uncertainty in these calculations. The best measurements of the neutron lifetime can currently achieve 0.36 s total uncertainties [6]. The neutron lifetime is a necessary component to determining the V_{ud} element of the CKM quark mixing matrix in the standard model (SM) of particle physics [7, 8]. Non-unitarity of the CKM matrix would signal new physics beyond the Standard Model. The best measurements of V_{ud} currently come from nuclear beta decay [7, 8], and as such are subject to nuclear structure corrections. A result from neutron beta decay would be a determination of V_{ud} free from these corrections. This is not sufficient for tests of the Standard Model via V_{ud} determinations, where a <0.3 s precision is necessary. In order to reach this precision regime, great care must be taken to understand and characterize the systematic uncertainties involved in the measurements. An independent and precise method for the evaluation of the efficiency of proton detectors used in “beam” determinations of the neutron lifetime is required to move forward.

1.1. Neutron Beta Decay

Neutron beta decay is the archetype for all nuclear beta decay processes. It makes for a very simple system to study the charged vector current component of the weak interaction as the neutron is a single nucleon, rather than a composite nuclear environment, making results easier to interpret. Within the Standard Model, neutron beta decay can (to a good approximation) be completely described by two quantities, g_V and g_A , which give the strength of the vector and axial-vector couplings in the weak interaction. Study of neutron beta decay includes several other observables, including the lifetime of the free

neutron as well as several correlation parameters. A measurement of the lifetime probes a linear combination of g_V^2 and g_A^2 , whereas several of the other correlation parameters give the ratio, g_A/g_V . Combining the measurements of multiple observables completely constrains the standard model parameters.

The neutron beta decay probability is given in Ref. [9] as:

$$dW \propto (g_V^2 + 3g_A^2)F(E_e) \left[1 + a \frac{\vec{p}_e \cdot \vec{p}_\nu}{E_e E_\nu} + \vec{\sigma}_n \cdot \left(A \frac{\vec{p}_e}{E_e} + B \frac{\vec{p}_\nu}{E_\nu} \right) \right] \quad (1)$$

The $(g_V^2 + 3g_A^2)$ term is proportional to the neutron lifetime, as it is the linear combination of the g_A and g_V couplings; whereas the a, A, B correlation coefficients can be used to extract $\lambda = \frac{g_A}{g_V}$, their ratio via:

$$A = -2 \frac{|\lambda|^2 + \text{Re}[\lambda]}{1 + 3|\lambda|^2} \quad B = -2 \frac{|\lambda|^2 - \text{Re}[\lambda]}{1 + 3|\lambda|^2} \quad a = \frac{1 - |\lambda|^2}{1 + 3|\lambda|^2} \quad (2)$$

Examining Eq. 1, the physical meaning of the correlation parameters is quite clear: A is the correlation between the initial spin of the neutron and the momentum of the outgoing electron, B is the analog for the anti-neutrino, and a is the correlation between the directions of the outgoing electron and anti-neutrino. The PDG value of λ is currently 1.2723 ± 0.0023 [10], derived primarily from A measurements. The final result from the UCNA collaboration [11] is consistent with this, but not yet incorporated into the PDG average. A scaling factor of 2.2 is at present assigned to the average uncertainty from the experiments. This is due to the fact that the most recent and precise measurements have shifted towards higher values of $|\lambda|$, resulting in a double peak, seen in Fig. 1. Forthcoming values by way of a measurements from aCORN [12] and Nab [13, 14] experiments will be a necessary high-precision check to the existing measurements.

1.2. Beam Method

The result of most recent extraction of the neutron lifetime via the ‘‘beam’’ method [15, 16] is called Beam Lifetime 1 (BL1) and is succeeded by the in-progress measurement, Beam Lifetime 2 (BL2). These experiments are done

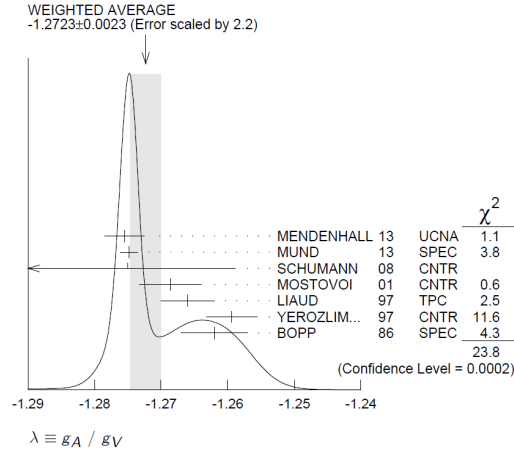


Figure 1: PDG Determination of λ . Currently used experimental values as well as the average and the scaling factor effect are shown.

at the National Institute of Standards and Technology in Gaithersburg, MD (NIST). This apparatus is one of a kind worldwide and is currently capable of achieving a 1 s lifetime measurement, which is the level of uncertainty in “storage” experiments.

Ion-implanted silicon detectors were used during BL1 and are, once again, being used in BL2 for proton detection. In the beta decay of cold neutrons (energies of order of 10s of meV), the daughter protons have a maximum of 760 eV of kinetic energy. This is not sufficient for detection, as approximately 10 keV is required to penetrate the dead layer of the detector. To address this, the proton detector in the experiment is held at a -30 kV potential, accelerating the particles into the detector. BL1 counted the protons using a discriminator threshold placed on the proton detector signal, meaning the waveform itself was not recorded. Protons are sometimes scattered from the detector back into the magnet volume, these particles will be guided and accelerated by the EM field back into the detector face. In this situation the detector will see no hits above threshold, or multiple hits from a single particle. The threshold method of proton counting will misclassify such events and the waveform data would

be unavailable for more detailed analysis. The calculation of the backscattering correction and uncertainty requires a series of measurements using different acceleration potentials as well as detectors with different dead-layer thicknesses. Essentially, BL1 calculated the neutron lifetime in configurations yielding different fractions of protons that backscatter (calculated via SRIM [17]) and extrapolated to zero backscattering. The current uncertainty associated with this process is 0.4 s and is unchanged from BL1 to BL2, as no improvements nor changes have been made.

It is likely that the discrepancy between the different determinations of the neutron lifetime are due to an unaccounted for (or improperly accounted for) systematic error in one or both approaches. The beam method relies on precise and accurate knowledge of the neutron and proton detector efficiencies. We propose a method for absolute proton detector calibration through coincidence measurements of electrons and protons from the laser-ionization of atomic hydrogen will address the question of hidden “unknowns” in the latter. Additionally, 60% of the existing 0.4 s uncertainty in the proton backscattering determination comes from the calibration of the detector with radioactive sources in-situ and is limited by a number of technical issues. A direct calibration will reduce this 0.24 s contribution to relatively negligible levels.

2. Proposed Method

The main objective of this publication is to provide a procedure for absolute detector calibration for both the existing and future proton detector designs. Some collaborations have built proton sources to attempt to characterize charged particle detectors. Such an approach is insufficient for lifetime determinations, as the initial flux cannot be measured down to each individual particle. Instead, using this method, protons and electrons would be detected in coincidence (as well as in singles mode) following a laser-induced ionization of hydrogen gas.

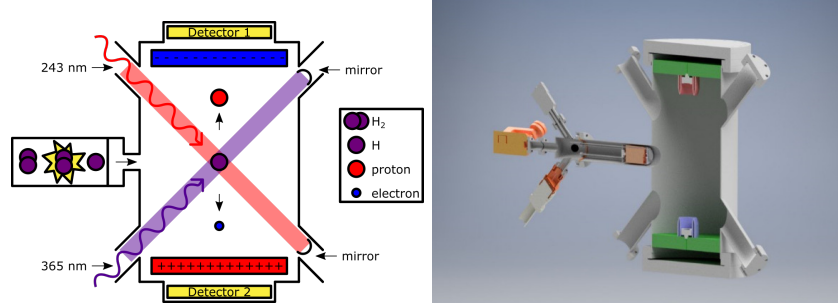


Figure 2: Graphic to illustrate the proposed apparatus. Left Panel: molecular hydrogen is disassociated into atomic hydrogen, which is then excited to the $2s$ state via laser excitation. A higher wavelength laser is then used to ionize the atoms. The resulting electrons and protons are accelerated by \pm potentials to identical ion-implanted silicon detectors. Right Panel: A notional Inventor model to illustrate the proposed apparatus. The two arms on the right may also include mirrors to reflect the light for additional efficiency. The red and blue objects are corona shields to supply the acceleration potentials to the detectors G10 disks are included for electrical isolation (green), but the HV isolation cages are not pictured.

2.1. Coincidence e - p detection

The proposed proton detector calibration apparatus is designed to use singles and coincidence detection of electrons and protons from ionization of hydrogen to calibrate both detectors (two BL2 detectors will be used). The efficiency of each detector is given as $\epsilon_1 \& \epsilon_2$, the rate of ionization of hydrogen is N_0 and the

number of particles detected in each detector is given by N_1 & N_2 . N_c represents the number of coincidences detected in the apparatus. Equation 3 shows how the measurements allow for the determination of the individual detector efficiencies.

$$\begin{aligned} N_1 &= N_0 \epsilon_1 & N_2 &= N_0 \epsilon_2 & N_c &= N_0 \epsilon_1 \epsilon_2 \\ \epsilon_1 &= \frac{N_c}{N_2} & \epsilon_2 &= \frac{N_c}{N_1} \end{aligned} \tag{3}$$

Today, an off-the-shelf atomic hydrogen [18] source can be obtained, removing the need to construct something to disassociate molecular hydrogen. Fig. 2 shows a schematic of the experimental setup. Atomic hydrogen is introduced using a commercially available source (such as the Tectra thermal hydrogen cracker [18]).

2.2. Laser Excitation Schemes

Ionizing an H atom requires 13.6 eV of energy. We propose ionizing the H atoms via a two step laser excitation scheme. First, we excite the atoms from the $n = 1$ ground state to $n = 2$ excited state which requires 10.2 eV of energy corresponding to one 122 nm photon or two 243 nm photons. The one photon transition to the $2p_{3/2}$ state is electric dipole allowed, while a two photon transition to the $2s_{1/2}$ state is required by selection rules [19]. Second, the excited atoms are then ionized by a commercially available 365 nm laser [20] which provides the remaining 3.4 eV of energy at threshold. The main technical challenge, recently overcome as will be described, is producing the deep UV excitation laser light.

A common technique to generate the 243 nm photons is frequency doubling 486 nm light using a nonlinear crystal such as beta barium borate (BBO) [21] or cesium lithium borate (CLBO) [22]. The 486 nm light itself can be produced directly by a dye laser [21] or alternatively by frequency doubling light at 972.5 nm produced by an external cavity laser diode system [23]. Recently, a frequency quadrupled laser system using Yb-doped fiber amplifiers produced watts of 243 nm light [24]. Furthermore, this state of the art laser system was used to

populate the 2s state of atomic hydrogen for a precision measurement of the 2s to 8d transition frequency in atomic hydrogen [25]. Finally, we expect that a frequency quadrupled 972.5 nm 5 W Ti:Sapphire laser would be capable of producing hundreds of mW of 243 nm light [26].

Alternatively, two groups have recently demonstrated a pulsed Lyman- α laser at 122 nm [27, 28]. The two schemes are similar and involve first the generation of 729 nm using a pulsed Ti:Sapphire laser which is subsequently frequency doubled using a lithium borate (LBO) nonlinear doubling crystal. The subsequent 364.5 nm light is frequency tripled using third harmonic generation in a Kr/Ar gas cell. Such a laser was recently used to laser cool antihydrogen at CERN [29].

2.3. Population Rate Equations

The fractional populations of the ground state n_g , excited state n_e , and ionized state n_i vary in location and time. We approximate the spatial dependence of the various rates by a time dependence assuming that all the H atoms are moving at a constant speed given by the mean thermal speed. In particular, the laser excitation rate is nonzero only during the time it takes the H atom to traverse the interaction region where the two lasers overlap with the H atomic beam. All other rates are independent of time although they may be electric field dependent, which we assume is spatially uniform. The rate equations that govern the populations under these assumptions are:

$$\dot{n}_g = -Rn_g + \frac{n_e}{\tau_e} \quad (4)$$

$$\dot{n}_e = +Rn_g - \frac{n_e}{\tau_e} - \Gamma_{\text{ion}}n_e \quad (5)$$

$$\dot{n}_i = +\Gamma_{\text{ion}}n_e \quad (6)$$

where $n_g + n_e + n_i = 1$, R is the laser excitation rate to the $n = 2$ state from the $n = 1$ ground state, τ_e is the lifetime of the excited state in an electric field, and Γ_{ion} is the photoionization rate from the excited state. It is straightforward to show that the E -field ionization rates from either state are negligibly small. If the drift time of the electrons to exit the interaction region is sufficiently

short, then the electron-ion recombination rate in the interaction region is also negligibly small.

2.4. Ion Population Fraction Estimates

Assuming that the atoms stay in the interaction region long enough for the laser excitation process to reach quasi-equilibrium (i.e. $1/\tau_e$ is the fastest rate) and that $n_e, n_i \ll n_g \rightarrow n_g \approx 1$, then the ionized population fraction can be estimated by:

$$n_i \approx R\tau_e\Gamma_{\text{ion}}t_{\text{int}} \quad (7)$$

where t_{int} is the effective time that atoms are in the interaction region. We assume the following parameters to estimate the rates and ion population fractions under two different laser excitation schemes:

- $P_{2\gamma} = 1$ W, CW power of the 243 nm two photon excitation laser [24]
- $w_{2\gamma} = 100$ μm , gaussian beam radius for the 243 nm laser
- $E_{\text{pulse}} = 1$ nJ, $\tau_{\text{pulse}} = 15$ ns, $\nu_{\text{rep}} = 10$ Hz, pulse energy, duration, and repetition rate for a 122 nm single photon excitation laser [27, 28]
- $w_{1\gamma} = 1$ mm, gaussian beam radius for the 122 nm laser [29]
- $P_{\text{ion}} = 1$ W, CW power of the 365 nm photoionization laser [20]
- $w_{\text{ion}} = 100$ μm , gaussian beam radius for the 365 nm laser
- $\ell_{\text{int}} = 2$ mm, length of interaction region
- $T = 2000$ K, temperature of H atomic beam [30, 31]
- $E_{\text{field}} = 3$ kV/cm

Assuming a gaussian laser beam and a Doppler-broadened atomic beam, the peak laser excitation rates can be estimated by [32]:

$$R_{2\gamma} = \left(\frac{2P_{2\gamma}}{\pi w_{2\gamma}^2 h\nu_{2\gamma}} \right) \left[\left(\frac{\sigma_{2\gamma}}{g(2\omega)I(\omega)} \right) \sqrt{\frac{m_e c^2}{2\pi k T \omega_{2\gamma}^2}} \left(\frac{2P_{2\gamma}}{\pi w_{2\gamma}^2} \right) \right] \quad (8)$$

$$= (121 \text{ } \mu\text{Hz}) \left[\frac{P_{2\gamma}}{1 \text{ W}} \right]^2 \left[\frac{100 \text{ } \mu\text{m}}{w_{2\gamma}} \right]^4 \sqrt{\frac{2000 \text{ K}}{T}} \quad (9)$$

$$R_{1\gamma} = \left(\frac{2E_{\text{pulse}}/\tau_{\text{pulse}}}{\pi w_{1\gamma}^2 h\nu_{1\gamma}} \right) \left[\pi r_e c f_{2p3/2} \sqrt{\frac{m_e c^2}{2\pi k T \nu_{1\gamma}^2}} \right] \quad (10)$$

$$= (5.33 \text{ kHz}) \left[\frac{E_{\text{pulse}}/\tau_{\text{pulse}}}{(1 \text{ nJ})/(15 \text{ ns})} \right] \left[\frac{1 \text{ mm}}{w_{1\gamma}} \right]^2 \sqrt{\frac{2000 \text{ K}}{T}} \quad (11)$$

$$\Gamma_{\text{ion}}^{2s,2p} = \left(\frac{2P_{\text{ion}}}{\pi w_{\text{ion}}^2 h\nu_{\text{ion}}} \right) \left[\sigma_{\text{ion}}^{2s,2p}(0) \right] \quad (12)$$

$$= \begin{bmatrix} (173 \text{ kHz})_{2s} \\ (158 \text{ kHz})_{2p} \end{bmatrix} \left[\frac{P_{\text{ion}}}{1 \text{ W}} \right] \left[\frac{100 \text{ } \mu\text{m}}{w_{\text{ion}}} \right]^2 \quad (13)$$

where the term in (\dots) is the photon flux (number of photons per unit time per unit area) and the term in $[\dots]$ is the laser interaction cross section. The full Stark-mixed excited state lifetimes for $E_{\text{field}} = 3 \text{ kV/cm}$ are $\tau_{2s} = \tau_{2p} = 3.19 \text{ ns}$. The interaction time is given by time needed for the atomic beam to traverse the interaction region for the two photon scheme $\tau_{\text{int}}(2 \text{ mm}, 2000 \text{ K}) = \ell_{\text{int}} \sqrt{\pi m_H / (8kT)} = 0.309 \text{ } \mu\text{s}$ or the pulse duration for the one photon scheme $\tau_{\text{int}} = \tau_{\text{pulse}} = 15 \text{ ns}$.

Assuming a thermal atomic beam temperature of $T = 2000 \text{ K}$ and a static electric field of $E_{\text{field}} = 3 \text{ kV/cm}$, the estimated ionization fraction for the two laser excitation schemes are $n_i^{2\gamma} = 2 \times 10^{-14}$ and $n_i^{1\gamma} = 4 \times 10^{-8}$. The 122 nm excitation laser scheme, although technically more challenging, provides a 10^6 higher ionization fraction due to the significantly higher photoexcitation cross section.

2.5. Ion Production Rate Estimates

The ion production rate can be estimated by $dN_i/dt = n_i dN/dt$ where dN/dt is the number of H atoms passing through the interaction region. A commercial H atomic beam source (HABS) produces a total output of 2×10^{15} atoms/s

with a central peak flux of 1.5×10^{13} atoms/cm²/s with a thermal velocity distribution corresponding to $T = 2000$ K [30, 31, 18]. Assuming a intersection cross sectional area of $\pi w_{\text{ion}}^2 = 3 \times 10^{-4}$ cm² and using this hot commercial HABS with $dN/dt = 5 \times 10^9$ atoms/s would result in about $dN_i^{2\gamma}/dt \approx 10$ ions per day for the two photon scheme and $dN_i^{1\gamma}/dt \approx 200$ ions per sec for the one photon scheme.

Recently a cryogenic HABS has been developed [33] and used for a precision measurement of the 2s to 8d transition frequency in atomic hydrogen [25]. This cryogenic source produces a total output of 10^{17} H atoms/s at $T = 6$ K. Assuming a similar angular distribution as the hot commercial HABS, we estimate $dN/dt = 2 \times 10^{11}$ atoms/s which would result in about $dN_i^{2\gamma}/dt \approx 2$ ions per sec for the two photon scheme and $dN_i^{1\gamma}/dt \approx 200k$ ions per sec for the one photon scheme. The increased ion production rates are due to both the increased atomic beam flux and the significantly smaller Doppler broadening at cryogenic temperatures.

In the case that a background rate is proving problematic, the light sources may be operated in pulsed mode. This would help by allowing the light source trigger to act as a time-zero for the cracking of the hydrogen. The electron and proton measurement windows could then be opened at a well defined time after $t=0$.

The electrons and protons will be accelerated using a ± 30 kV potential to the detectors on either side of the vacuum chamber. This is essentially replicating the proton detection arm of the BL1/2 apparatus twice (for positive and negative charge detection). In the lifetime experiment itself, the protons are guided to the detector using the magnetic field, which is not present in this proposed apparatus. The simulation shown in Fig. 3 creates a proton-electron pair at the center of the apparatus from a hydrogen atom whose velocity is 6000 m/s (determined by the temperature of the hydrogen cracker). The particles see a 60 kV electric field across a distance of 20 cm between the detectors. Fig. 3 shows the area of the proton and electron hits. The smallest detectors used in BL2 have a diameter of 19.6 mm, meaning the initial hits of particles should

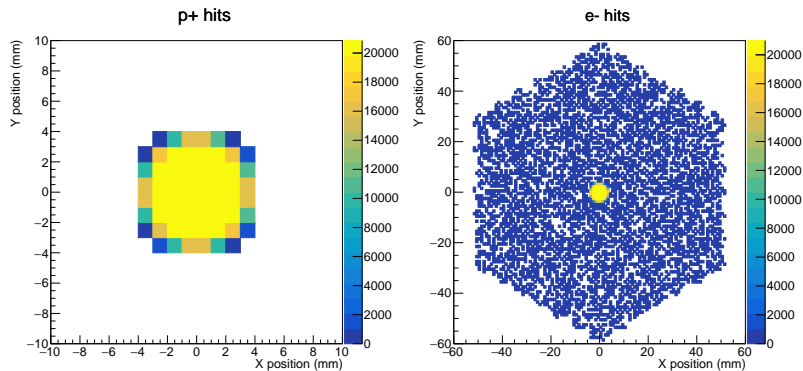


Figure 3: Preliminary results from a Geant4 simulation of proton and electron transport. Left Panel: A density plot showing the area of proton hits on the detector. The centroid will be offset in x by a few mm in the real device due to the initial momentum of hydrogen exiting the cracker. Right Panel: A density plot showing the area of electron hits on the detector as simulated in Geant4. The initial hit is always in the yellow central area. The wider area of hits are secondary and tertiary electron back-scatters from the detector face. Both the proton hit area and the initial hit area for electrons are well within the smallest detector size the apparatus is expected to test (19.6 mm diameter).

not fall outside the active area of the detector. The silicon detectors will scatter a fraction of incoming charged particles back into the drift area after absorbing some initial energy deposit. The back-scattered particles will decelerate into the potential region and be re-accelerated into the detector. It is shown in Fig. 3 that the electrons frequently scatter laterally as well, causing the subsequent hits to increase in radius from the center of the detector. The Protons do not show this behavior. The detector interaction is handled using the Livermore low energy physics package [34] included in Geant4.

Additional Geant4 simulations were performed, throwing optical photons at the detectors using the wavelengths of interest. This simulation was designed to test the device in a running mode, with protons, electrons and photons being thrown simultaneously. The study indicates that photons do not cause additional energetic deposits in the detector material. Shown in Fig. 4 is an energy spectrum of proton and electron hits from two different Geant4 simulations, one

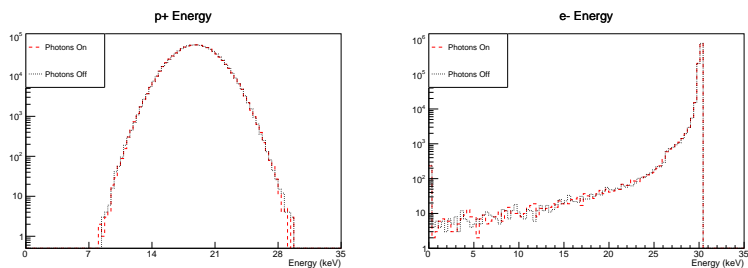


Figure 4: Preliminary results from a Geant4 simulation of proton and electron transport. Protons and electrons were thrown with coincident optical photons to simulate the chamber being illuminated by the wavelengths necessary to split the atomic hydrogen. No significant contribution to the number of hits nor the hit energy spectra is observed when optical photons are included in the simulation (dashed line) compared to when they are not (dotted line).

includes optical photons in the particle gun the other does not. No significant differences in total number of hits, or the energy distribution of hits is observed. The optical photon gun was tested in two configurations, positioned in the center of the device pointed normal to the detector face, and positioned 2mm from the detector with an incident angle on the silicon of 30 deg. Neither of these scenarios produced noticeable differences in the hit count nor energy spectrum of electron and proton hits. A highly absorptive coating will be painted on the inside of the apparatus to minimize the bouncing of optical photons around the chamber, in the true setup the lights are also not pointed directly at the detectors. This simulation was meant to represent a pessimistic case where neither of those factors were included.

3. Summary

The method proposed above would constitute vital part of the fundamental neutron physics program. To reach the precision where neutron measurements can be used to test the Standard Model require resolving the discrepancy in the neutron lifetime results from different measurement methods. The mounting of future experiments with low goal uncertainties demand that systematic

effects are well understood. Accurate proton detection and absolute detector calibration is a crucial part of this future.

References

- [1] F. E. Wietfeldt, G. L. Greene, The neutron lifetime, *Rev. Mod. Phys.* 83 (2011) 1173–1192.
- [2] H. Abele, The neutron. its properties and basic interactions, *Prog. Part. Nucl. Phys.* 60 (2008) 1 – 81.
- [3] P. A. R. Ade, et al., Planck 2013 results. XVI. Cosmological parameters, *Astron. Astrophys.* 571 (2014) A16. [arXiv:1303.5076](#), [doi:10.1051/0004-6361/201321591](#).
- [4] F. Iocco, G. Mangano, G. Miele, O. Pisanti, P. D. Serpico, Primordial nucleosynthesis: From precision cosmology to fundamental physics, *Phys. Rep.* 472 (2009) 1–76. [doi:10.1016/j.physrep.2009.02.002](#).
- [5] K. M. Nollett, G. Steigman, Bbn and the cmb constrain light, electromagnetically coupled wimps, *Phys. Rev. D* 89 (2014) 083508. [doi:10.1103/PhysRevD.89.083508](#)
URL <http://link.aps.org/doi/10.1103/PhysRevD.89.083508>
- [6] F. M. Gonzalez, E. M. Fries, C. Cude-Woods, T. Bailey, M. Blatnik, L. J. Broussard, N. B. Callahan, J. H. Choi, S. M. Clayton, S. A. Currie, M. Dawid, E. B. Dees, B. W. Filippone, W. Fox, P. Geltenbort, E. George, L. Hayen, K. P. Hickerson, M. A. Hoffbauer, K. Hoffman, A. T. Holley, T. M. Ito, A. Komives, C.-Y. Liu, M. Makela, C. L. Morris, R. Musedinovic, C. O’Shaughnessy, R. W. Pattie, J. Ramsey, D. J. Salvat, A. Saunders, E. I. Sharapov, S. Slutsky, V. Su, X. Sun, C. Swank, Z. Tang, W. Urich, J. Vanderwerp, P. Walstrom, Z. Wang, W. Wei, A. R. Young, Improved neutron lifetime measurement with UCN τ , *Phys. Rev. Lett.* 127 (2021) 162501. [doi:10.1103/PhysRevLett.127.162501](#)
URL <https://link.aps.org/doi/10.1103/PhysRevLett.127.162501>
- [7] J. C. Hardy, I. S. Towner, Superallowed $0^+ \rightarrow 0^+$ nuclear beta decays: A

new survey with precision tests of the conserved vector current hypothesis and the standard model, *Physical Review C* 79 (2009) 055502.

- [8] J. C. Hardy, I. S. Towner, Superaligned $0^+ \rightarrow 0^+$ nuclear β decays: 2014 critical survey, with precise results for V_{ud} and CKM unitarity, *Phys. Rev. C* 91 (2) (2015) 025501. [arXiv:1411.5987](#), [doi:10.1103/PhysRevC.91.025501](#).
- [9] J. D. Jackson, S. B. Treiman, H. W. W. Jr, Possible tests of time reversal invariance in beta decay, *Physical Review* 106 (1957) 517–521.
- [10] C. Patrignani, et al., Review of Particle Physics, *Chin. Phys.* C40 (10) (2016) 100001.
- [11] M. A. P. Brown, et al., New result for the neutron β -asymmetry parameter A_0 from UCNA (2017). [arXiv:1712.00884](#).
- [12] F. Wietfeldt, et al., aCORN: An experiment to measure the electron - antineutrino correlation in neutron decay, *Nucl. Instr. Meth. Phys. Res. A* 611 (2009) 207 – 210. [doi:10.1016/j.nima.2009.07.064](#).
- [13] D. Počanić, et al., Nab: Measurement principles, apparatus and uncertainties, *Nucl. Instr. Meth. Phys. Res. A* 611 (2009) 211 – 215. [doi:10.1016/j.nima.2009.07.065](#).
- [14] S. Baeßler, J. D. Bowman, S. Penttilä, D. Počanić, New precision measurements of free neutron beta decay with cold neutrons, *J. Phys. G* 41 (11) (2014) 114003. [doi:10.1088/0954-3899/41/11/114003](#).
- [15] J. S. Nico, et al., Measurement of the neutron lifetime by counting trapped protons in a cold neutron beam, *Phys. Rev. C* 71 (2005) 055502.
- [16] A. Yue, M. Dewey, D. Gilliam, G. Greene, A. Laptev, et al., Improved Determination of the Neutron Lifetime, *Phys.Rev.Lett.* 111 (22) (2013) 222501. [arXiv:1309.2623](#), [doi:10.1103/PhysRevLett.111.222501](#).

- [17] J. F. Ziegler, Stopping range of ions in matter, computer code available at www.srim.org (2008).
- [18] Tectra, Atomic hydrogen source, <http://tectra.de/sample-preparation/atomic-hydrogen-source/>.
- [19] C. J. Foot, Atomic physics, Oxford University Press, Oxford, UK, 2005.
- [20] TOPTICA Photonics AG, Products:uvrgb solutions, [Online; accessed 31-October-2023] (2023).
URL <https://www.toptica.com/products/single-frequency-lasers/uv-rgb-solutions>
- [21] C. J. Foot, P. Hannaford, D. N. Stacey, C. D. Thompson, G. H. Woodman, P. E. G. Baird, J. B. Swan, G. K. Woodgate, Observation of the $1s$ - $2s$ transition in atomic hydrogen in an atomic beam, *Journal of Physics B: Atomic, Molecular and Optical Physics* 23 (11) (1990) L203. doi:10.1088/0953-4075/23/11/003.
URL <https://dx.doi.org/10.1088/0953-4075/23/11/003>
- [22] Z. Burkley, C. Razor, S. F. Cooper, A. D. Brandt, D. C. Yost, Yb fiber amplifier at 972.5 nm with frequency quadrupling to 243.1 nm, *Applied Physics B* 123 (1) (2016) 5. doi:10.1007/s00340-016-6583-9.
URL <https://doi.org/10.1007/s00340-016-6583-9>
- [23] N. Kolachevsky, J. Alnis, S. D. Bergeson, T. W. Hänsch, Compact solid-state laser source for $1s$ - $2s$ spectroscopy in atomic hydrogen, *Phys. Rev. A* 73 (2006) 021801. doi:10.1103/PhysRevA.73.021801.
URL <https://link.aps.org/doi/10.1103/PhysRevA.73.021801>
- [24] Z. Burkley, A. D. Brandt, C. Razor, S. F. Cooper, D. C. Yost, Highly coherent, watt-level deep-uv radiation via a frequency-quadrupled yb-fiber laser system, *Appl. Opt.* 58 (7) (2019) 1657-1661. doi:10.1364/AO.58.001657.
URL <https://opg.optica.org/ao/abstract.cfm?URI=ao-58-7-1657>

- [25] A. D. Brandt, S. F. Cooper, C. Rasor, Z. Burkley, A. Matveev, D. C. Yost, Measurement of the $2s_{1/2} - 8d_{5/2}$ transition in hydrogen, *Phys. Rev. Lett.* 128 (2022) 023001. doi:10.1103/PhysRevLett.128.023001.
URL <https://link.aps.org/doi/10.1103/PhysRevLett.128.023001>
- [26] S. Degenkolb, Optical magnetometry using multiphoton transitions, Ph.D. thesis, University of Michigan, Ann Arbor (2016).
- [27] J. M. Michan, G. Polovy, K. W. Madison, M. C. Fujiwara, T. Momose, Narrowband solid state vuv coherent source for laser cooling of antihydrogen, *Hyperfine Interactions* (235) (2015) 29–36. doi:10.1007/s10751-015-1186-0.
URL <https://link.springer.com/article/10.1007/s10751-015-1186-0>
- [28] G. Gabrielse, B. Glowacz, D. Grzonka, C. D. Hamley, E. A. Hessels, N. Jones, G. Khatri, S. A. Lee, C. Meisenhelder, T. Morrison, E. Nottet, C. Rasor, S. Ronald, T. Skinner, C. H. Storry, E. Tardiff, D. Yost, D. M. Zambrano, M. Zielinski, Lyman- α source for laser cooling antihydrogen, *Opt. Lett.* 43 (12) (2018) 2905–2908. doi:10.1364/OL.43.002905.
URL <https://opg.optica.org/ol/abstract.cfm?URI=ol-43-12-2905>
- [29] C. Baker, et al., Laser cooling of antihydrogen atoms, *Nature* (592) (2021) 35–42. doi:10.1038/s41586-021-03289-6.
URL <https://www.nature.com/articles/s41586-021-03289-6>
- [30] U. Bischler, E. Bertel, Simple source of atomic hydrogen for ultrahigh vacuum applications, *Journal of Vacuum Science & Technology A* 11 (2) (1993) 458–460. arXiv:https://pubs.aip.org/avs/jva/article-pdf/11/2/458/11853287/458_1_1_online.pdf, doi:10.1116/1.578754.
URL <https://doi.org/10.1116/1.578754>
- [31] C. Eibl, G. Lackner, A. Winkler, Quantitative characterization of a highly effective atomic hydrogen doser, *Journal of Vacuum Science & Technology A* 16 (5) (1998) 2979–2989. arXiv:<https://pubs.aip.org/avs/>

`jva/article-pdf/16/5/2979/7432502/2979_1_online.pdf`, doi:10.1116/1.581449.

URL <https://doi.org/10.1116/1.581449>

- [32] A. E. Siegman, Lasers, revised edition, University Science Books, Melville, NY, USA, 1986.
- [33] S. F. Cooper, A. D. Brandt, C. Rasor, Z. Burkley, D. C. Yost, Cryogenic atomic hydrogen beam apparatus with velocity characterization, Review of Scientific Instruments 91 (1) (2020) 013201. arXiv:https://pubs.aip.org/aip/rsi/article-pdf/doi/10.1063/1.5129156/13992302/013201_1_online.pdf, doi:10.1063/1.5129156.
URL <https://doi.org/10.1063/1.5129156>
- [34] L. N. Lab, Livermore low energy electromagnetic physics, code Documentation available: <https://geant4.web.cern.ch/node/1619> (2003).
- [35] J. H. Tung, A. Z. Tang, G. J. Salamo, F. T. Chan, Two-photon absorption of atomic hydrogen from two light beams, J. Opt. Soc. Am. B 3 (6) (1986) 837–848. doi:10.1364/JOSAB.3.000837.
URL <https://opg.optica.org/josab/abstract.cfm?URI=josab-3-6-837>
- [36] A. Burgess, Tables of hydrogenic photoionization cross-sections and recombination coefficients, Memoirs of the Royal Astronomical Society 69 (1965) 1.
- [37] L. D. Landau, E. M. Lifshitz, Quantum Mechanics, Non-relativistic Theory, Second edition, revised and enlarged, Pergammon Press, Oxford, U.K., 1965.
- [38] M. H. Rice, R. H. Good, Stark effect in hydrogen*, J. Opt. Soc. Am. 52 (3) (1962) 239–246. doi:10.1364/JOSA.52.000239.
URL <https://opg.optica.org/abstract.cfm?URI=josa-52-3-239>

- [39] R. J. Damburg, V. V. Kolosov, An asymptotic approach to the stark effect for the hydrogen atom, *Journal of Physics B: Atomic and Molecular Physics* 11 (11) (1978) 1921. doi:10.1088/0022-3700/11/11/009.
URL <https://dx.doi.org/10.1088/0022-3700/11/11/009>
- [40] J. Spitzer, Lyman, J. L. Greenstein, Continuous Emission from Planetary Nebulae, *Astrophysical Journal* 114 (1951) 407. doi:10.1086/145480.
- [41] A. Kramida, Yu. Ralchenko, J. Reader, and NIST ASD Team, NIST Atomic Spectra Database (ver. 5.10), [Online]. Available: <https://physics.nist.gov/asd> [2023, October 30]. National Institute of Standards and Technology, Gaithersburg, MD. (2022).
- [42] G. Breit, E. Teller, Metastability of Hydrogen and Helium Levels., *Astrophysical Journal* 91 (1940) 215. doi:10.1086/144158.
- [43] W. E. Lamb, R. C. Retherford, Fine structure of the hydrogen atom. part i, *Phys. Rev.* 79 (1950) 549–572. doi:10.1103/PhysRev.79.549.
URL <https://link.aps.org/doi/10.1103/PhysRev.79.549>